Combining AFM and Acoustic Probes to Reveal Changes in the Elastic Stiffness Tensor of Living Cells

ARTICLE *in* BIOPHYSICAL JOURNAL · OCTOBER 2014

Impact Factor: 3.97 · DOI: 10.1016/j.bpj.2014.07.073

5 AUTHORS, INCLUDING:

Xuegen Zhao
The University of Manchester
26 PUBLICATIONS **166** CITATIONS
SEE PROFILE

Alexandre Carisey
Baylor College of Medicine
10 PUBLICATIONS **234** CITATIONS
SEE PROFILE

Christoph Ballestrem
The University of Manchester
52 PUBLICATIONS **3,412** CITATIONS
SEE PROFILE

Brian Derby
The University of Manchester
305 PUBLICATIONS **4,944** CITATIONS
SEE PROFILE

Combining AFM and Acoustic Probes to Reveal Changes in the Elastic Stiffness Tensor of Living Cells

N. Nijenhuis[†‡], X. Zhao[†], A. Carisey[‡], C. Ballestrem[‡] and B. Derby[†*]

[†] School of Materials, University of Manchester, Oxford Road, Manchester, M13 9PL, UK.

[‡] Wellcome Trust Centre for Cell-Matrix Research, Faculty of Life Sciences, University of Manchester, Oxford Road, Manchester, M13 9PT, UK.

*Corresponding author: brian.derby@manchester.ac.uk

Running Title: Combining AFM and Acoustic Probes

Keywords: Acoustic Microscopy, Atomic Force Microscopy, Mechanical Properties, Young's Modulus, Shear Modulus, Bulk Modulus, Poisson Ratio

Combining AFM and Acoustic Probes to Reveal Changes in the Elastic Stiffness Tensor of Living Cells. N. Nijenhuis, X. Zhao, A. Carisey, C. Ballestrem and **B. Derby**, *Biophys. J.* **107**, 1502–1512 (2014).

DOI: 10.1016/j.bpj.2014.07.073

Abstract

Knowledge of how the elastic stiffness of a cell affects its communication with its environment is of fundamental importance for the understanding of tissue integrity in health and disease. For stiffness measurements it has been customary to quote a single parameter quantity, e.g. Young's modulus, rather than the minimum of two terms of the stiffness tensor required by elasticity theory. In this study we use two independent methods (Acoustic Microscopy and AFM Nanoindentation) to characterise the elastic properties of a cell and thus determine two independent elastic constants. This allows us to explore in detail how the mechanical properties of cells change in response to signalling pathways that are known to regulate the cell's cytoskeleton. In particular we demonstrate that altering the tensioning of actin filaments in NIH 3T3 cells has a strong influence on the cell's shear modulus but leaves its bulk modulus unchanged. In contrast, altering the polymerisation state of actin filaments influences bulk and shear modulus in a similar manner. In addition, we can use the data to directly determine the Poisson ratio of a cell and show that in all cases studied it is less than but very close to 0.5 in value.

Introduction

In multicellular organisms, cells interact mechanically with the local environment and studying their response to external stresses and strain is important for the understanding of their behaviour in health and disease. Cells are dynamic structures and react to external mechanical stimuli that determine cell fate (1, 2). Cells also react by changing their own internal architecture, which in turn leads to the alteration of mechanical properties of the cells themselves. For example, it has been shown that breast tumourigenesis is accompanied by extracellular matrix stiffening (3) and cell stiffness can be a signature for tumours (4).

The mechanical behaviour of a cell is governed by its complex internal structure, of which the cytoskeleton of filamentous actin (F-actin), intermediate filaments and microtubules is believed to be the most important. This is in turn controlled by filament cross linking, motor and regulatory proteins. In the literature, as reviewed by both Lim et al. (5) and Kasza et al. (6), there are two alternative approaches that can be used to predict the mechanical behaviour of cells: a "bottom up" approach that models the behaviour of a cell as a network of polymer fibres, and a "top down" approach that seeks to consider and model a cell as a discrete entity. The bottom up approach applies the principles of polymer physics to describe the behaviour of filamentary networks (7-9) and as such may give greater insight into the mechanisms that generate the mechanical properties of cells. However, in order to make useful numerical predictions from these models, it is normal to describe the predicted behaviour by using a continuum formulation such as elasticity or viscoelasticity. The top down approach seeks to define the behaviour of a cell by directly determining a constitutive law that relates the action of external forces to local displacements, normally based on data from whole cell deformation experiments, and thus empirically formulate the mechanical behaviour within a preselected continuum formulation. Although the top down approach lacks a direct physical interpretation, the continuum formulation can be used with powerful computational tools such as the finite element method to produce predictions of cell behaviour such as cell contractility and migration (10, 11). Thus, although there are two distinct approaches to analysing or predicting the mechanical response of a cell, the end result in both cases is the derivation of a relationship between mechanical force and displacement that replaces the internal structure of a cell by an effective medium or continuum. We note that more sophisticated models of cells that mimic a variation in mechanical properties within a single cell, still use a continuum formulation but with the continuum properties showing spatial variation in properties (10, 12).

The simplest constitutive law that can be used to model cell behaviour is elastic behaviour where the deformation is proportional to the applied stress and is recovered once stress is removed. Time dependent deformation of a cell can be modelled using more complex constitutive laws, two such examples are given below:

1) *Viscoelastic* behaviour has been used to model the behaviour of cells (13). This is often used to model the behaviour of solid polymers where deformation can occur by the relative displacement of polymer chains. Lim noted that an elastic model of a cell can be related to time dependent viscoelastic models through the correspondence principle (5).

2) *Poroelastic* (or biphasic) behaviour, shows a time dependency controlled by the flow of liquid through nanoscale pores and channels in response to local differences in pressure and the deformation rate limited by its viscosity. Poroelasticity is used to model the deformation of some soft tissues (14) and has been suggested as applicable to the deformation of cells. given the large amount of fluid present in the cytoplasm (15).

However it is difficult to conclusively distinguish between poroeleastic behaviour and viscoelastic behaviour without probes for fluid migration during cell deformation. A number of reviews of cell mechanical behaviour state that over reasonably short time scales, of a few seconds or less, cell behaviour can be adequately described by an elastic model (5, 6, 12). Thus describing cell behaviour using a simple elastic constitutive law is appropriate and will be used in the rest of this work.

In the literature, cell stiffness is commonly described by a single parameter, typically Young's modulus or the shear modulus. However, cells are 3-dimensional (3D) objects and in organisms most cell types are normally embedded in an extracellular matrix. Hence their resistance to deformation must be described in 3D Cartesian space. From simple deformation theory it can be shown that in a homogeneous and isotropic medium, an arbitrary 3D elastic deformation consists of two independent components, a change in volume and a change in shape or shear (16). Thus in order to describe mechanical responses to forces in 3D a minimum of two independent elastic constants are required, one to represent the resistance to a change in shape and the second its resistance to a change in volume.

Cell Elastic Properties

Structural rigidity is believed to be controlled by the cell cytoskeleton, which consists of three interconnected networks of polymer molecules comprising actin filaments, microtubules and intermediate filaments. Cells can regulate intracellular tension and cell stiffness through actomyosin contractility (17, 18); the actomyosin machinery is linked via adapter proteins to transmembrane adhesion receptors, the integrins, which bind components of the extracellular matrix proteins. Microtubules are thought to resist the compression load formed by actomyosin tension (19). Chemicals that interfere with the structural polymers of the cytoskeleton are known to strongly influence cell mechanical properties. The actin filament network can be disrupted through the action of cytochalasin D or latrunculin B hereby reducing the stiffness of cells (20). Microtubule disrupting drugs, *e.g.* nocodazole, conversely are associated with an increase in actin polymerisation and bundling (21).

In this study we are using a top down approach and assume that the properties of the cell can be adequately modelled using a constitutive law modelling elastic behaviour. We assume that the mechanical properties of the cell can be modelled as an isotropic elastic continuum described by a symmetrical 4^{th} rank tensor, represented in matrix notation by (22):

$$\begin{pmatrix} C_{11} & C_{12} & C_{12} & 0 & 0 & 0 \\ - & C_{11} & C_{12} & 0 & 0 & 0 \\ - & - & C_{11} & 0 & 0 & 0 \\ - & - & - & C_{44} & 0 & 0 \\ - & - & - & - & C_{44} & 0 \\ - & - & - & - & - & C_{44} \end{pmatrix} \quad (1)$$

For an isotropic material $C_{44} = (C_{11} - C_{12})/2$, hence there are two independent elastic constants (16).

For ease of interpretation, it is often more convenient to describe the elastic properties in terms of two conventional (or engineering) elastic constants; *i.e.* any pair of the following: Young's modulus, *E*, Poisson's ratio, ν, shear modulus, *G*, or the bulk modulus, *K*, with:

$$E = \frac{(C_{11} - C_{12})(C_{11} + 2C_{12})}{(C_{11} + C_{12})} \tag{2a}$$

$$\nu = \frac{C_{12}}{(C_{11} + C_{12})} \tag{2b}$$

$$G = \frac{(C_{11} - C_{12})}{2} \tag{2c}$$

$$K = \frac{(C_{11} + 2C_{12})}{3} \tag{2d}$$

Conversely, it is possible to fully describe the elastic properties of a cell if any two of the above elastic constants are measured.

In practice most measurements of the elastic properties of cells are made using a single experimental technique accessing one elastic constant. To get round this, the Poisson's ratio is usually assumed to be 0.5, which would be the case if the cell was incompressible. However, Poisson's ratio is rarely measured with biological materials and the value of $\nu = 0.5$ is assumed by analogy with synthetic compliant polymers and elastomers (4, 23-26). Note that this value implies that the cell is incompressible and although this may be a reasonable approximation to cell behaviour, the laws of solid mechanics accept a value of 0.5 for Poisson's ratio as an upper bound to behaviour if a material is isotropic and homogeneous, with real materials showing values slightly smaller than 0.5.

There have been a few published studies that have reported Poisson ratio values for single cells. Shin used an indentation method to compress individual of osteoblast-like cells, their analysis reported a best fit to data if $\nu = 0.37 \pm 0.03$ (27). Charras and Horton combined an AFM study of cell deformation with finite element analysis to explore the influence of Poisson ratio in the range 0.2 - 0.5 on their measured mechanical property data (28). Although no direct measurement of Poisson's ratio was made, Charras noted that the value of Poisson ratio selected (assumed) made a significant difference to the apparent stiffness of the cell. Mahaffy et al used AFM nanoindentation to determine the mechanical properties of NIH 3T3 fibroblast cells using indentation models for thin compliant films bonded to a stiffer substrate. They found that the data is consistent with mechanical models using Poisson's ratio values in the range 0.4 - 0.5 (29). Although both the studies of Charras and Mahaffy report a value for both Young's modulus and Poisson's ratio using a mechanical model of the indentation process, it is unlikely that these are truly independent measures because in each case they are derived from a single mechanical measurement. Trickey et al measured the mechanical properties of chondrocyte cells via micropipette aspiration and reported $\nu = 0.38 \pm 0.06$ (30). Finally Ma et al studied the deformation of stem cell aggregates and deduced that a reasonable value is $\nu = 0.45$ (31). Both Trickey and Ma used a finite element model to predict the deformation of the cells or cell aggregates in response to a force. In both these reports, Poisson's ratio was obtained through an optimisation process in which the influence of changes in the value of Poisson's ratio and Young's modulus used in the model were compared to the overall observed deformation of a cell or cell aggregate. In all cases the major criticism of the methodology is the use of a single deformation mode to determine two independent elastic constants. From this published data we conclude that there is no agreed value for Poisson's ratio of an individual cell nor has there been any study as to whether this elastic constant changes with induced changes to a cell's cytoskeleton.

Measuring the Elastic Properties of Cells

There are a number of experimental techniques that can be used to measure the mechanical properties of cells including: aspiration of cells into capillaries (32), stretching of cells by optical tweezers (33), nanoindentation with atomic force microscopy (AFM) (23) and measuring acoustic wave velocity (34). Two independent mechanical measurements of a cell allow two independent components of the elasticity tensor to be determined. Here the techniques we use are:

1. measuring the acoustic wave velocity using scanning acoustic microscopy (SAM) images,
2. nanoindentation using an AFM.

Combining indentation and acoustic wave velocity measurements have been previously used to measure the elastic properties of homogeneous solid materials (35, 36).

The SAM is used to measure the mean longitudinal acoustic wave velocity, v_{long}, in a cell (34, 37). This is directly related to C_{11} with (16):

$$v_{long} = \sqrt{\left(\frac{C_{11}}{\rho}\right)} \tag{3}$$

where ρ is the mean density of the cell. The second experimental method analyses the elastic response of a cell to spherical indentation carried out with an AFM, using Hertz's solution for the indentation of an elastic half space by a sphere (23). An animal cell has an elastic stiffness that is many orders of magnitude smaller than most solid materials used in indentation experiments and thus the indentation can be modelled as if by a rigid sphere. In which case the displacement, δ, as a function of indentation load, P, is described by:

$$\delta = \left(\frac{9P^2}{16RE^{*2}}\right)^{1/3} \tag{4a}$$

here R is the radius of the indenting sphere and E^* is the contact (or reduced) Young's modulus, defined by

$$E^* = \frac{E}{1-\nu^2} \tag{4b}$$

where E and ν are Young's modulus and Poisson's ratio of the cell respectively. In terms of the components of the stiffness tensor, equation 3b can be written:

$$E^* = \frac{(C_{11}-C_{12})(C_{11}+C_{12})}{C_{11}} = \frac{\left(C_{11}^2-C_{12}^2\right)}{C_{11}} \tag{5}$$

Measuring the acoustic wave velocity gives direct access to the C_{11} component of the stiffness tensor (equation 3), which measures the resistance to volume change of a cell under pressure. AFM nanoindentation measures the contact Young's modulus of the cell and as can be seen from equations 2a, 2c and 5 this is related to the difference between the C_{11} and C_{12} components of the stiffness tensor, which defines the resistance of the cell to shear deformation. Therefore, by combining measurements of the acoustic wave velocity in a cell with measurements of the contact modulus determined using the AFM, it is possible to measure independently a cell's resistance to shear deformation and volume change and from

these data calculate the isotropic elastic stiffness tensor of a cell and hence any of the cell's conventional elastic constants without the need for prior assumptions.

Thus, by measuring two independent elastic constants, we provide a better insight into the 3D mechanical response of a cell than can be achieved using a single elastic constant. This in turn allows the exploration of how different modifications of cell function separately affect cell resistance to change in volume and resistance to shear deformation. We illustrate this through investigating how the RhoA pathway influences cell mechanical behaviour through the action of two downstream pathways that influence myosin-mediated cell contractility and formin (mDia)-mediated actin polymerisation, both of which are important for coordinated cell motility (figure 1) (38, 39).

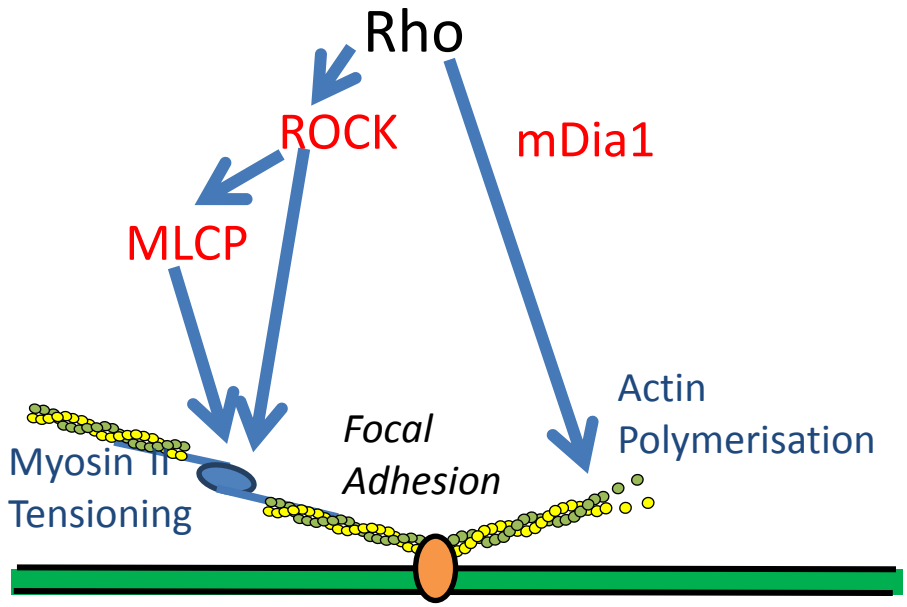

Figure 1 Schematic diagram, after Riveline et al (38), showing the effect of Rho on cell mechanical properties through the activation of two pathways: ROCK dependent and mDia1 dependent. The ROCK dependent pathway tensions the actin fibres through myosin II–driven cell contractility either directly or indirectly, via myosin light chain phosphatase (MLCP). The mDia1 dependent pathway activates actin polymerization, or possibly influences the organization of the actin network and microtubules.

Materials and Methods

Cells, Media, and Reagents

NIH3T3 mouse fibroblasts (LGC-ATCC, Teddington, UK) were cultured at 37ºC in Dulbecco's modified Eagle's medium (Sigma-Aldrich, Poole, UK) supplemented with 10% foetal bovine serum (Lonza, Cologne, Germany), 2 mM L-glutamine, and nonessential amino acids (all from Sigma-Aldrich). Nocodazole and ROCK-inhibitor Y-27632 were used at 1 µM and 100 µM respectively (both from Sigma-Aldrich). For acoustic wave and AFM measurements NIH3T3 mouse fibroblasts were plated on glass bottom dishes (MatTek Corporation, Ashland MA, USA) that were coated for 1h at room temperature with 10 µg/ml fibronectin diluted in PBS and rinsed twice with PBS.

Transfection

For transient transfections of NIH3T3 cell line, Lipofectamine and Plus reagents (Life Technologies, Paisley, UK) were used according to the manufacturer's instructions on cells seeded 24 hours before transfection in 6-well dishes. The plasmid encoding fluorescently labelled mDia1ΔN3 construct was from the A. Bershadsky lab (Weizmann Institute of Science, Rehovot, Israel). Glass bottom dishes (MatTek Corporation, Ashland MA) were coated for 1h at room temperature with 10 μg/ml fibronectin diluted in PBS and rinsed twice with PBS. Three hours after transfection, cells were plated in complete DMEM and allowed to spread in the glass bottom dishes 24 hours before the experiment.

Immunofluorescence

After 24 hours, cells were fixed with 4% (wt/vol) paraformaldehyde and permeabilised with 0.5% (vol/vol) Triton X-100 (both from Sigma-Aldrich) diluted in PBS. Samples were subsequently incubated for 1 hour with an antibody directed against β-tubulin (clone DM1A, Sigma-Aldrich) directly conjugated with FITC. Staining for actin was performed at the same time using Texas-Red-X-conjugated phalloidin. Samples were observed on a Deltavision RT microscope (Applied Precision, Issaquah, WA, USA) using a 100x NA 1.40 Uplan Apo objective (Zeiss, Cambridge, UK) and 86000v2 or 86006 filter sets (Chroma Technology, Bellows Falls VT, USA). Images were collected using a Coolsnap HQ CCD (Photometrics, Tucson, AZ, USA) camera, converted and analysed using Fiji software (40). Raw images were subjected to signal re-scaling using linear transformation for display purposes in the figures.

Acoustic microscopy

Acoustic measurements were made using a KSI 2000 microscope (PVA TePla Analytical Systems GmbH; Herborn, Germany) with a custom data acquisition and control system. In brief, the system operates at 1GHz, with quasi monochromatic tone bursts, of burst length ≈ 20 ns and a repetition rate of ≈ 500 kHz. The lens is initially focused at the substrate surface by monitoring the maximum output of the received signal with a gate setting optimized for in-focus signals. The lens was then raised 4 μm away from the substrate and a stack of images was taken at different z-positions commencing from this height towards the substrate surface with a step-size of 0.1 μm over a range of 5 μm. It took approximately 13 minutes to acquire a full stack of 50 images. The gray scale value for every pixel (*x, y* position) was extracted from all the images at each *z* position to form a *V(z)* curve. Analyzing each *V(z)* curve provides a measure of the acoustic phase across the specimen, from which the mean acoustic wave velocity at each pixel location can be determined using a procedure described in detail elsewhere (37). The height of each cell was also measured using the interference rings visible in each acoustic image. The accuracy of this measurement was compared with AFM measurements of cell height and these were found to be consistent. Acoustic attenuation through a single cell is small and does not influence the acoustic wave velocity measurement. The acoustic wave velocity data was obtained by determining an average value from a linescan across the width of the cell nucleus region.

Atomic force microscopy

Cell elasticity was probed at the nucleus region of the spread out-cells with an atomic force microscope (AFM) (Nanowizard, CellHesion 200; JPK Instruments, Berlin, Germany), installed on a fluorescence microscope (Axiovert 200M; Zeiss, Jena, Germany). Tipless AFM cantilevers (Arrow TL1, k = 0.03 N/m; NanoWorld, Neuchâtel, Switzerland) were modified by attaching 4.5 μm diameter polystyrene beads at their ends. Modification of the cantilevers was done by Novascan, Ames, USA. Cantilevers were calibrated in the medium filled

chambers using the thermal noise method (41) prior to the experiments. Cells were indented at the nucleus region with an approach speed of 5 μm/s until a loading force of 2 nN was reached. Each cell was deformed in this way for three times at the same position with about 30 s intervals between indentations. The measured force-indentation depth curves (see figure S1 in the Supporting Material for an example) were fitted using built-in JPK software, implemented with the Hertz model for a spherical indenter, giving the Young's modulus *E*. The Poisson ratio of the cells was taken as 0.5 for the purpose of this calculation. Only the first 0.4 μm of indentation was used for determination of *E*, this is approximately 10% of the height of the cells and was chosen to minimise any effect of substrate stiffness (42), in addition only curves for which *E* was independent of indentation depth were used. For subsequent processing of data the influence of the assumed Poisson's ratio was eliminated by back calculating the contact modulus.

Statistical analysis

For both acoustic wave velocity measurements and contact modulus determination, a large number of experiments were repeated among the population of cells studied to determine mean values and standard error of the mean (SE). The error bars in the figures indicate ±SE. Statistical significance was determined using a 2-tailed T-test with the level of significance set as probability $p < 0.05$.

Results and Discussion

Actin Tensioning Influences Shear Modulus but not Bulk Modulus

In non-muscle cells the motor protein myosin IIA is identified as the myosin involved in actomyosin regulated tension. Its activation state is regulated by phosphorylation (43) of its light chain mediated by the Rho-associated protein kinase (ROCK) pathway (17, 44). Downstream of RhoA, ROCK controls the myosin light chain kinase (MLCK) by regulating myosin light chain (MLC) phosphorylation, which is important for actomyosin-mediated cell contractility (figure 1). Another important effector of RhoA is mDia1, which when rendered active induces actin polymerization and increases microtubule stabilization. Thus RhoA plays, not only via the ROCK but also via the mDia1 pathway, an important role in the regulation of cell mechanical properties (figure 1) (38, 45). To examine the contribution of ROCK on the stiffness of NIH3T3 cells, we blocked it by adding the protein kinase inhibitor Y-27632 (46). Treatment of cells with this drug, through the absence of myosin II mediated tensioning, led to the complete disassembly of actin stress fibres (figures 2a and 2b).

Figures 2c and 2d show SAM images produced from NIH3T3 control cells and cells treated with Y-27632. The mean cell height (± SD) was 3.84 ± 0.68 μm for the control samples and 4.17 ± 0.77 μm after treatment with Y-27632, this difference is statistically significant ($p = 0.008$). Parallel AFM measurements on a number of cells were carried out to determine cell height and these were consistent with the SAM data. Figures 2a and 2b show the corresponding fluorescence microscopy images of cells, stained to reveal bundled filamentous actin; here, in the absence of tensioning, the actin is significantly more disorganised. The SAM data can be converted into acoustic wave (sound) velocity following the procedure of Zhao *et al.* (37) and is shown in figure 2e. For reference the acoustic wave velocity in the PBS medium used for acoustic microscopy is approximately 1490 ms^{-1} (37) and this is similar to the values of 1495 ±7 ms^{-1} and 1483 ms^{-1} reported by Rapoport et al (47) and Baddour et al (48), respectively. Hence there is a significant difference between the acoustic wave velocity in the cell and in the surrounding media.

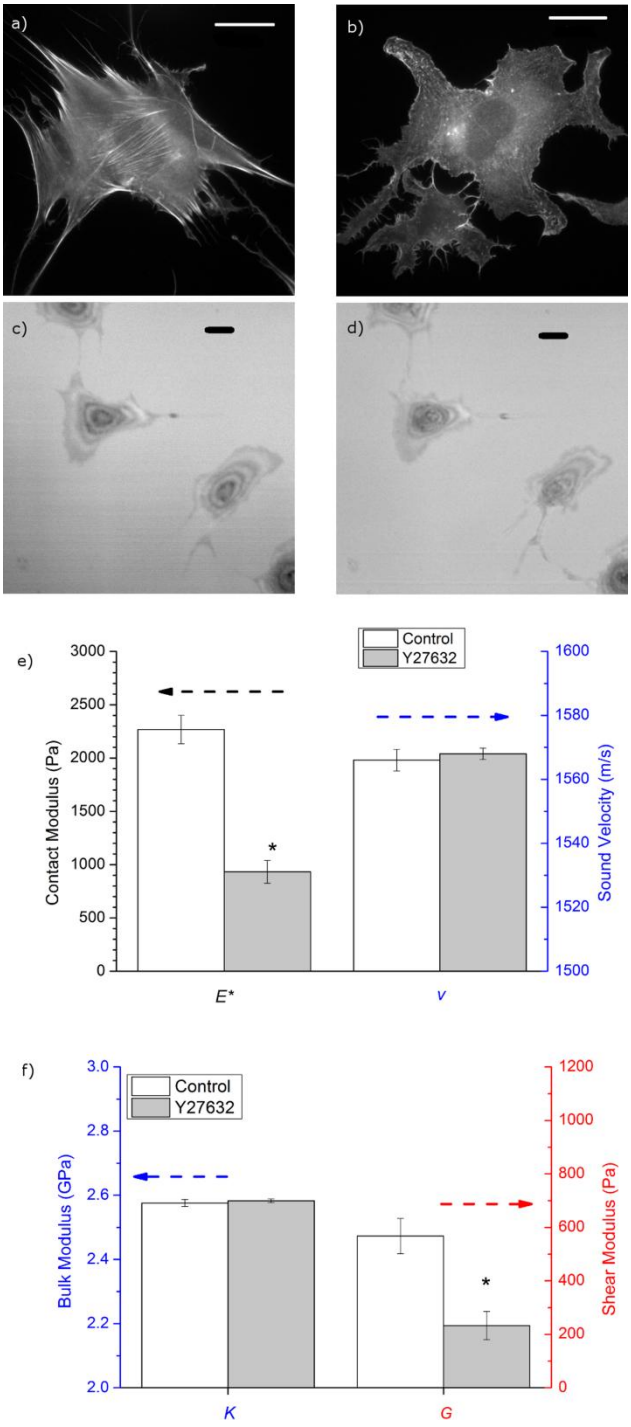

Figure 2 SAM and AFM experiments on populations of cells treated with Y-27632 and a control population. a) Filamentous actin structure in a control NIH3T3 cell showing regular straight, tensioned filaments called stress fibres. b) Highly disorganised actin filamentary structure observed after treatment with Y-27632. c) SAM image showing characteristic interference rings from a typical control NIH3T3 cell. d) NIH32T3 cell after treatment with Y-27632 showing a larger number of interference rings and a more raised profile. In all images the scale bar indicates 10 μm. e) Mean (± S.E.) acoustic wave velocity (control: n = 27, Y-27632: n = 51) and contact elastic modulus (control: n = 92: Y-27632: n = 27). f) Computed bulk modulus (K) and shear modulus (G). In all cases * indicates a statistically significant difference ($P < 0.05$) between treated and control populations.

The uncertainty in the exact height of a cell is probably the greatest cause of intrinsic error in measuring acoustic wave velocity. The error associated with uncertainties in cell height was calculated by Zhao (figure 8 in reference (37)) and is approximately 2 ms^{-1} per 0.1 μm uncertainty in cell height for the cells in this study. Zhao reported a variation of about ± 3 ms^{-1} in the acoustic wave velocity measured across the nucleus region of a single cell and we estimate that this is approximately what would be expected from uncertainties in local cell height. The standard deviation of the acoustic wave velocity measured in each cell population ranged from about 12 - 23 ms^{-1} (Table S1, in the Supporting Material). Thus the variation within each group of cells measured was always significantly greater than the intrinsic uncertainty in the method used to measure the acoustic wave velocity in an individual cell. In order to acquire the full data set the cells are imaged over a period of about 13 minutes. Because the elastic response is related to an acoustic excitation, the timescale of the mechanical response is unrelated to the time taken for image acquisition.

Our acoustic data gives results similar to the acoustic wave velocities obtained by Kundu *et al.* for XTH2 cells using 1 Ghz acoustic waves with a different analysis methodology (1500 - 1700 ms^{-1}) (34) , and by Taggart *et al.* for a range of human derived cells (1522 - 1537 ms^{-1}) using 40 MHz acoustic waves (49). Our improved analytical method uses phase information and has been shown to reduce the scatter and uncertainty in the acoustic wave velocity compared with other published methods, hence explaining the lower levels of experimental scatter when our data is compared with that of Kundu or Taggart (37). We note that the addition of Y-27632 does not significantly change the acoustic wave velocity ($p = 0.3$).

The AFM measurements (figure 2e) show a significant decrease in the contact modulus after the addition of Y-27632 ($p < 10^{-6}$). This apparent discrepancy with the SAM data may appear surprising but we will show that this is consistent with changes in the tensorial representation of the elastic properties of cells. Note that the statistical scatter of the two measurements are quite different, with the acoustic wave velocity measurement showing a much lower variation as a fraction of the measurement value than the corresponding AFM data. We interpret this as demonstrating a greater intrinsic variability in the AFM measurement of cell stiffness. This is almost certainly caused by error in the identifying the contact between the AFM tip and the cell surface, which will lead to uncertainties in the precise value of δ in equation 3a (50). When the tip is immersed there are further hydrodynamic effects which may additionally impede surface detection (51). Further uncertainties may occur when determining the AFM cantilever spring constant. We have calculated the cantilever spring constant using the thermal fluctuation method (41), as used by many research groups, however this may lead to errors in excess of 30% of the measured value (52). Note that these errors will be between groups, because a single AFM cantilever was used to measure each individual cell population studied.

The data used in this study and in the studies subsequently reported are presented in tabular form in Table S1 in the Supporting Material. If we compare our AFM cell stiffness data with that in the literature (a convenient review is presented by Kuznetsova et al (53)), it is clear that our data (control cell population mean Young's modulus ± S.D, $E = 1520 \pm 646$ Pa) is similar, in both magnitude and reported experimental scatter, to that reported in other studies of the stiffness of fibroblast cells.

This data can be used with equations 2 - 5 to determine the two independent terms of the isotropic stiffness tensor, if the density of the cell is known (see Table S2 in the supporting material). There have been relatively few studies of the density of individual cells under physiological conditions, chiefly because of the difficulty of making such measurements. Anderson et al used high molecular weight solute to vary the density of cell suspending

media with minimal effect on osmotic pressure and used a range of such fluids to study the centrifuge assisted migration of cells (54). This method was used to study how the density of CHO cells varied through the cell cycle, to obtain an estimated density (± S.D.) of 1052 ± 3 kgm^{-3} with any variation in density during the cycle being significantly lower than the standard deviation. Anderson et al used their calculations to comment on density measurements by other workers, who had used similar methods but had not corrected for osmotic effects. They concluded that, because the density measurements obtained for rabbit thymocytes, LKID, and HeLa cells were all within 6 kgm^{-3} of the CHO data, there was considerable uniformity in the density of mammalian cells. Grover et al have developed a method to measure the mass of individual cells using a micromachined resonator and coupled this with optical measures of cell volume to calculate cell density (55). Unfortunately their published data only reports the density of erythrocytes and lymphocytes.

The density of a cell measured in suspension may be different from that of a cell adhered to a substrate but in the absence of any data to confirm this we have used the values determined from isolated cells in suspension. Thus, on the basis of Anderson's analysis, we assume a constant cell density value of 1050 kgm^{-3} throughout this study. We use this to compute the engineering elastic constants of shear and bulk modulus, G and K respectively (figure 2f). The error values of the elastic constants were calculated using conventional error propagation laws from the standard error reported for the data obtained using AFM and acoustic microscopy (Table S2). We believe that any systematic error from differences in the values of the cell density are unlikely to be much larger than the population error.

Here we should note that we are constructing a stiffness tensor using data measured with deformation time constants that differ by several orders of magnitude. It is well known that viscoelastic materials show a time dependent deformation behaviour that can result in quite different values of apparent Young's or shear modulus depending on the time scale of the deformation. However, the bulk modulus shows a much smaller influence of deformation rate (56). This is probably because the mechanism for viscoelastic behaviour is related to polymer deformation through chain sliding. If the deformation is primarily a volume change there will be no mechanism for polymer chain sliding and the elastic properties will be independent of loading rate. We postulate that because the acoustic wave velocity is related to the C_{11} modulus (equation 3), it too will show little variation with loading rate and thus we can combine the AFM data with the acoustic microscope data, despite the acoustic data operating at a rate of 1 GHz and the AFM data being acquired in the effective range 1 - 10 Hz.

The change in the bulk and shear modulus illustrates how the action of Y-27632 influences the cells resistance to volume change and shear. From these figures we can see that the resistance to volume change is unaffected within statistical limits but the resistance to shear has been reduced dramatically. This behaviour is interpreted as an effect of the deactivation of the myosin motors, which eliminates the tensioning of the actin filaments but does not influence the quantities of the cytoskeleton structural polymers (actin and microtubules) nor promote any structural change (*e.g.* crosslinking) and thus the elastic compressibility is unchanged. However, removing the tensioning of the actin filaments has allowed the deformation of the cell to occur easily under shear loading with no change in volume. This is in agreement with data from *in vitro* experiments on f-actin and myosin II gels by Mizuno et al where shear stiffness was only present when the actin filaments were tensioned by the myosin (57). Such behaviour is fully consistent with a "tensegrity" model for the cytoskeleton where structural integrity is maintained by tensioning of structural fibres (19). In the absence of such tensioning there will be significantly reduced resistance to shear (shape change), while there will be no difference to any resistance to change in volume.

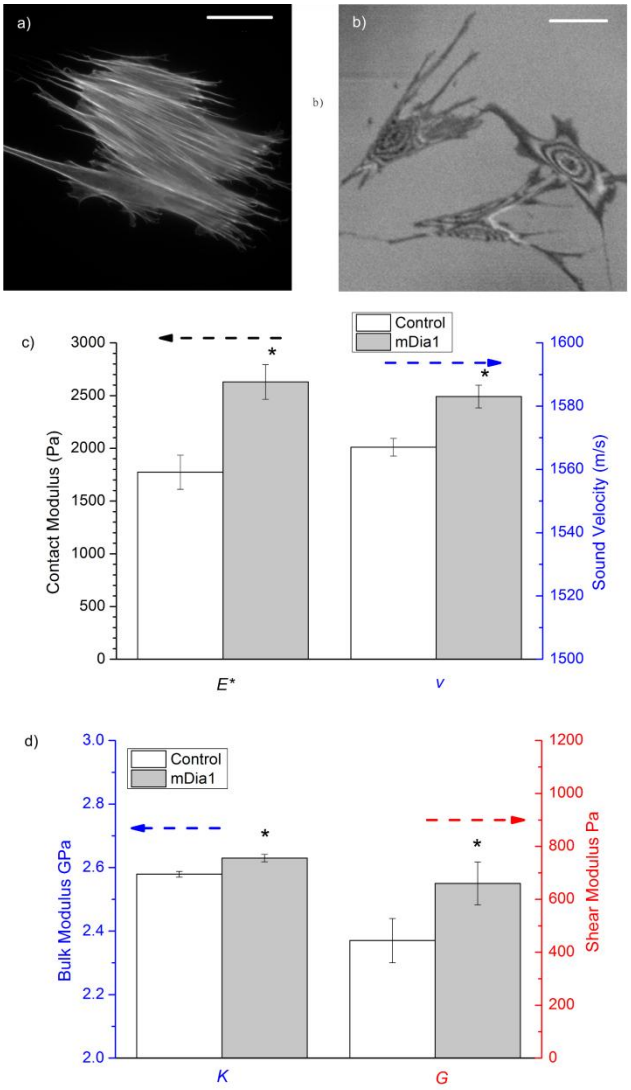

Figure 3 SAM and AFM experiments on populations of cells transfected with mDia1ΔN3 and a control population. a) NIH3T3 cell transfected with mDia1ΔN3 packed with a dense network of actin stress fibres; scale bar indicates 10 μm. b) SAM image showing interference rings from transfected NIH3T3 cells; scale bar indicates 20 μm. c) Mean ± S.E. acoustic wave velocity (control: n = 38, mDia1ΔN3: n = 45) and contact elastic modulus (control: n = 30, mDia1ΔN3: n = 55). d) Computed Mean ± SE bulk modulus (*K*) and shear modulus (*G*). In all cases * indicates a statistically significant difference ($P < 0.05$) between treated and control populations.

Actin Polymerisation Influences both Shear and Bulk Modulus

To examine the effect of increased actin polymer on NIH3T3 cells we expressed a constitutively active form of the formin mDia1 (mDia1ΔN3) in NIH3T3 cells, which has been shown to dramatically promote actin polymerisation in cells (45, 58). Cells expressing mDia1ΔN3 have a characteristic bipolar shape with the dense actin filaments following the long axis of the cell (figure 3a). The characteristic shape of the mDia expressing cells can be readily identified by the SAM image (figure 3b); in this case the cells have a mean height of 4.12 ± 0.81 μm which is slightly higher than the mean height of the control population ($p = 0.033$). In figure 3c the transfected cells show a small (< 20 ms^{-1}) but statistically significant increase in acoustic wave velocity ($p = 4.9 \times 10^{-4}$). This is consistent with previous *in vitro* studies of actin gels (59) where small increases in acoustic wave velocity were observed with increasing polymerisation of dilute actin gels. The transfected cells also display a significant (and relatively larger) increase in the contact modulus ($p = 2.0 \times 10^{-4}$), also in figure 3c. This data has been used to compute the bulk and shear modulus of the control and transfected cell populations (figure 3d). From this it is clear that the mDia1ΔN3 induced actin polymerisation has resulted in a significant increase in both the bulk and shear modulus. We interpret this result as showing that by increasing the filamentous fraction of actin the cell becomes more rigid, and less compressible. This is supported by the predictions obtained using classical rule of mixtures estimates of the elastic properties of composites, (60) where an increase in the fraction of the stiffer component in a composite structure (in this case actin filaments) leads to an increase in both the shear modulus and Young's modulus.

Influence of Microtubule Disruption Countered by Actin Polymerisation

Nocodazole is commonly used to disrupt microtubules. Thus one might expect that disrupting microtubules in cells would reduce cell stiffness and shear resistance (19). Figures 4a and 4b show that the network of microtubules revealed through staining a control cell population has disappeared after treatment with nocodazole. Figures 4c and 4d show that the actin stress fibres are slightly increased by the action of nocodazole but in this case the mean height of the cell in the SAM images (figure 4e) is 2.72 ± 0.49 μm and significantly smaller than the control cell population ($p < 10^{-6}$). Despite the disruption of microtubules, there is a small but statistically significant increase in acoustic wave velocity ($p = 5.9 \times 10^{-3}$) and also a significant increase in contact elastic modulus ($p = 1.0 \times 10^{-5}$) (figure 4f). From this data both the bulk and shear modulus values also show a significant increase (figure 4g). These results are similar to those reported by Wu (11), who also measured an increase in cell stiffness in the presence of nocodazole. It has been shown that the disruption of microtubules leads to the activation of RhoA (61), thereby activating downstream ROCK leading to myosin activation and endogenous mDia leading to increased actin polymeristation (Figure 1). It is thus these mechanisms that seem to compensate for the presumed reduction in cell stiffness that should result from microtubule disruption. We note that in the case of the nocodazole treated cells, the AFM indentation, 0.4 μm, is > 10% of the cell height at the nucleus, hence the increase in stiffness recorded by the AFM may be partly caused by the influence of the substrate "sensed" when indenting thin sections (42).

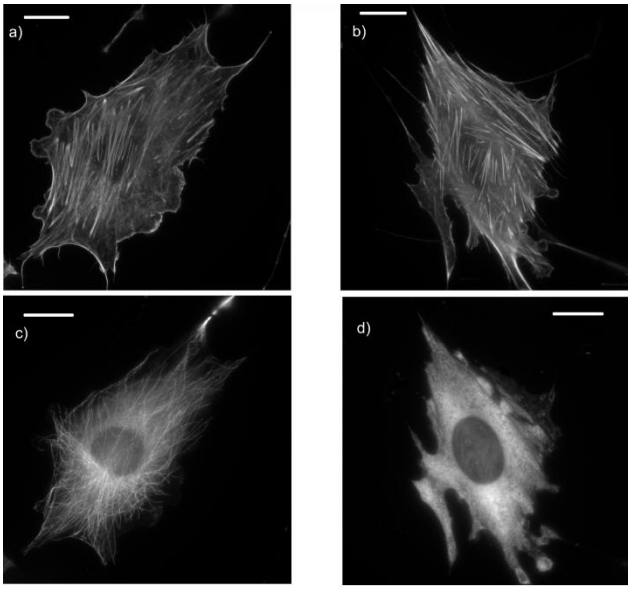
a)
b)
c)
d)

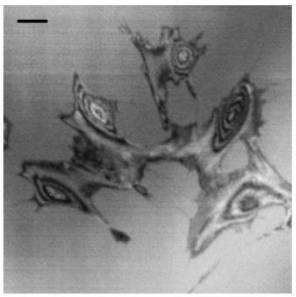
e)

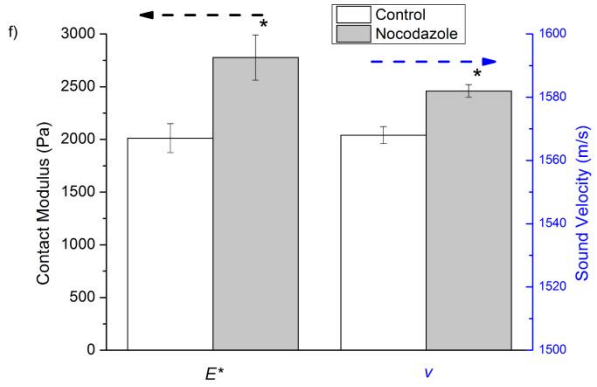
f)
Control
Nocodazole
Contact Modulus (Pa)
Sound Velocity (m/s)
3000
2500
2000
1500
1000
500
0
1600
1580
1560
1540
1520
1500
*
*
E*
v

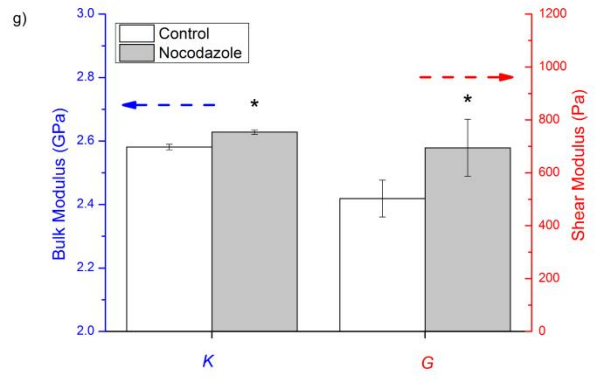
g)
Control
Nocodazole
Bulk Modulus (GPa)
Shear Modulus (Pa)
3.0
2.8
2.6
2.4
2.2
2.0
1200
1000
800
600
400
200
0
*
*
K
G

Figure 4 SAM and AFM experiments on populations of NIH3T3 cells treated with nocodazole and a control population. a) NIH3T3 cell in control condition stained to reveal microtubules. b) After treatment with nocodazole the microtubule structure is no longer revealed by the stain, indicating severe disruption. c) NIH3T3 cell in control condition stained to reveal actin. d) After treatment with nocodazole, actin filaments are clearly present in a similar amount to the control and well aligned. In images a-d the scale bars indicate 10 μm. e) SAM image of the cells after treatment with nocodazole, the presence of several interference rings show that the cells have maintained a 3D shape; scale bar indicates 20 μm. f). Mean (± S.E.) acoustic wave velocity (control: n = 34, nocodazole: n = 47) and contact elastic modulus (control: n = 39, nocodazole: n = 40). g) Computed mean ± S.E. bulk modulus (K) and shear modulus (G). In all cases * indicates a statistically significant difference ($P < 0.05$) between treated and control populations.

Poisson's Ratio of a Cell is very Close to 0.5

Finally we consider the Poisson's ratio of the cells. Most continuum models of cell mechanical behaviour take the cell's Poisson's ratio of the cell to be $\nu = 0.5$, which assumes the cell to be incompressible. Indeed, most measurements of the Young's modulus of a cell using Hertzian indentation models have taken this value of Poisson's ratio (4, 23-26). A small number of studies have assumed a different value with Charras and Mason (28) and Kelly et al (62) using $\nu = 0.3$ and $\nu = 0.37$, respectively.

Our results show that the cell has a finite bulk modulus (see figures 2f, 3d and 4g), albeit orders of magnitude greater than the shear modulus. All our results indicate that $K >> G$ for all control cells and treated cells investigated, hence from equation 5 we expect Poisson's ratio to be very close to 0.5. Thus in order to explore the variation in Poisson's ratio, ν, it is more convenient to plot the deviation of its calculated value from 0.5. Figure 5 shows the value of $0.5 - \nu$ for all the cell populations studied. The value for the error reported for our Poisson's ratio values was determined using the standard laws for error propagation through equations 2 - 5. This apparently low value can be better understood with reference to equation 5b where it is clear that any deviation from the incompressible value of $\nu = 0.5$ is a measure of the difference between C_{11} and C_{12}. The *difference* between these elastic constants is independent of the measured acoustic wave velocity and is instead determined by our AFM data for E^*, as seen clearly in equation 4. Thus the error in our estimation of Poisson's ratio is related to the error in measuring E^* divided by the value of C_{11}.

Poisson's ratio was calculated for the control and treated populations for all three cell treatments studied. In all cases the measured Poisson's ratio is very close to 0.5, with $(0.5 - \nu) < 1.5 \times 10^{-7}$. The addition of Y-27632 leads to the value closest in magnitude to 0.5, this is consistent with the very low resistance to shear induced by the absence of myosin activity. Indeed, from equations 2b and 2c it is clear that if $\nu = 0.5$, then $G = 0$, which is a characteristic feature of a liquid. There is to our knowledge only one published study on the influence of cell treatment on Poisson's ratio by Maniotis et al (63). They state that they measure an "apparent Poisson's ratio" by anchoring a cell through puncturing the membrane prior to capillary deformation and subsequently measuring the displacement within an area of approximately 10 μm^2. They find a low value of the apparent Poisson's ratio (approximately 0.25) in a control population that increases dramatically when cytoskeleton modifying drugs

are added, in contrast to the very small change in value reported here. This discrepancy may in part be explained by the very large displacements used in Maniotis's study, in which case some of the deformation may be outside the elastic regime and represent permanent deformation of the cell. Indeed they comment that some of their observed change in Poisson's ratio can be explained by fluid loss from the cell. Our Poisson's ratio data indicates that cell volume is conserved during deformation and this behaviour is consistent with a high fluid content within the cell.

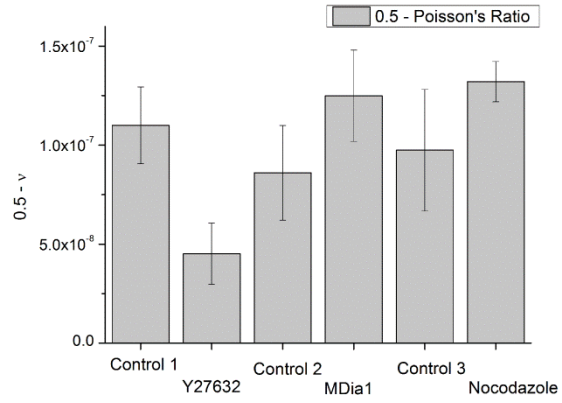

Figure 5 Deviation of the value of Poisson's ratio from the incompressible limit ($\nu = 0.5$) for the cell populations studied after a number of treatments.

Conclusions

In order to model the behaviour of a cell as an elastic body a minimum of two elastic constants are required, even if the cell is represented as a homogeneous, isotropic continuum. These two properties are needed because the small scale elastic deformation of a body can be decomposed into a change in volume and a change in shape. By using two independent methods to characterise the mechanical behaviour of a population of cells, SAM and AFM, the first of which is sensitive to changes in volume and the second to changes in shape, we have been able to determine two independent components of the stiffness tensor of a cell type and hence calculate two independent elastic constants without any prior assumptions concerning their mechanical behaviour. Using this approach we have been able to determine accurately the following information about the resistance of cells to relatively small scale deformations with time constants < 1s.

We have demonstrated that Poisson's ratio of NIH3T3 cells is very close to, but slightly less than, 0.5, deviating from this value by $< 1.5 \times 10^{-7}$ for all conditions studied. This shows that a cell is very close to incompressible in behaviour, which is consistent with a high free flowing fluid level in the cytoplasm.

By monitoring the changes in the two elastic properties after modifying the cytoskeleton of NIH3T3 cells, we identify how changes to the composition and organisation of the cytoskeleton contribute to the resistance of a cell to deformation, by separating the effect on volume change from that of shape change. The bulk modulus of the cell depends on the quantities of the structural components of the cytoskeleton and is sensitive to the total actin filament content. However, in order to resist a change in shape (shear deformation) the actin

filaments must be under tension and in the absence of tension the cell shows a dramatic reduction in shear modulus but not in its bulk modulus. A similar behaviour is seen with the Poisson's ratio measured for the cell. In all cases this is slightly smaller than 0.5 but it approaches 0.5 when the actin fibres are not tensioned. A Poisson's ratio of 0.5 is accompanied by a shear modulus of zero and is thus incompatible with any resistance to shape change. These results are consistent with the tensegrity model for the influence of the cytoskeleton on cell stiffness (19). However, by providing evidence for a structure consisting of a rigid tensioned framework within a liquid cytoplasm, it also suggests that a more sophisticated model for cell behaviour, that would be needed for large deformation or long time studies, will need to account for the redistribution of fluid within a deforming cell and this would likely be a biphasic or poroelastic constitutive law.

This study shows that by combining two independent probes of the mechanical properties of cells we are able to provide a more complete picture as to how changes in the cell cytoskeleton influence its mechanical behaviour. The approach we have used assumes a simple elastic model of cell behaviour but, by identifying two independent components of the stiffness tensor, it allows for the 3-dimensional nature of the mechanical interactions of cells with the environment. We believe that this more complete description of cell mechanical behaviour will enable a better understanding of the pathology of disease and cancer at the cellular level.

Acknowledgements

BD acknowledges funding from the BBSRC (BB/G000336/1). CB acknowledges the BBSRC (BB/G004552/1) and Wellcome Trust (088785/Z/09/Z) for funding of this work.

References

1. Discher, D. E., P. Janmey, and Y. L. Wang. 2005. Tissue cells feel and respond to the stiffness of their substrate. Science 310:1139-1143.

2. Butcher, D. T., T. Alliston, and V. M. Weaver. 2009. A tense situation: forcing tumour progression. Nat. Rev. Cancer 9:108-122.

3. Levental, K. R., H. Yu, L. Kass, J. N. Lakins, M. Egeblad, J. T. Erler, S. F. T. Fong, K. Csiszar, A. Giaccia, W. Weninger, M. Yamauchi, D. L. Gasser, and V. M. Weaver. 2009. Matrix Crosslinking Forces Tumor Progression by Enhancing Integrin Signaling. Cell 139:891-906.

4. Cross, S. E., Y.-S. Jin, J. Rao, and J. K. Gimzewski. 2007. Nanomechanical analysis of cells from cancer patients. Nat. Nanotechnol. 2:780-783.

5. Lim, C. T., E. H. Zhou, and S. T. Quek. 2006. Mechanical models for living cells - A review. J. Biomech. 39:195-216.

6. Kasza, K. E., A. C. Rowat, J. Liu, T. E. Angelini, C. P. Brangwynne, G. H. Koenderink, and D. A. Weitz. 2007. The cell as a material. Curr. Opin. Cell Biol. 19:101-107.

7. Das, M., F. C. MacKintosh, and A. J. Levine. 2007. Effective medium theory of semiflexible filamentous networks. Phys. Rev. Lett. 99:038101.

8. Vaziri, A., and A. Gopinath. 2008. Cell and biomolecular mechanics in silico. Nat. Mater. 7:15-23.

9. Gardel, M. L., K. E. Kasza, C. P. Brangwynne, J. Liu, and D. A. Weitz. 2008. Mechanical Response of Cytoskeletal Networks. Biophysical Tools for Biologists, Vol 2: in Vivo Techniques. Methods Cell Biol. 89:487-519.

10. Deshpande, V. S., R. M. McMeeking, and A. G. Evans. 2006. A bio-chemo-mechanical model for cell contractility. Proc. Nat. Acad. Sci. U.S.A. 103:14015-14020.

11. Kim, J. S., and S. X. Sun. 2009. Continuum modeling of forces in growing viscoelastic cytoskeletal networks. J. Theor. Biol. 256:596-606.

12. Heidemann, S. R., and D. Wirtz. 2004. Towards a regional approach to cell mechanics. Trends Cell Biol. 14:160-166.

13. Karcher, H., J. Lammerding, H. D. Huang, R. T. Lee, R. D. Kamm, and M. R. Kaazempur-Mofrad. 2003. A three-dimensional viscoelastic model for cell deformation with experimental verification. Biophys. J. 85:3336-3349.

14. Korhonen, R. K., M. S. Laasanen, J. Toyras, R. Lappalainen, H. J. Helminen, and J. S. Jurvelin. 2003. Fibril reinforced poroelastic model predicts specifically mechanical behavior of normal, proteoglycan depleted and collagen degraded articular cartilage. J. Biomech. 36:1373-1379.

15. Mitchison, T. J., G. T. Charras, and L. Mahadevan. 2008. Implications of a poroelastic cytoplasm for the dynamics of animal cell shape. Semin. Cell Dev. Biol. 19:215-223.

16. Landau, L., and E. Lifshitz. 1986. Theory of Elasticity. Butterworth Heinemann, Oxford, UK.

17. ChrzanowskaWodnicka, M., and K. Burridge. 1996. Rho-stimulated contractility drives the formation of stress fibers and focal adhesions. J. Cell Biol. 133:1403-1415.

18. Ridley, A. J., and A. Hall. 1992. The Small GTP-Binding Protein Rho Regulates the Assembly of Focal Adhesions and Actin Stress Fibres in Response to Growth Factors. Cell 70:389-399.

19. Ingber, D. E. 2003. Tensegrity I. Cell structure and hierarchical systems biology. J. Cell Sci. 116:1157-1173.

20. Wakatsuki, T., B. Schwab, N. C. Thompson, and E. L. Elson. 2001. Effects of cytochalasin D and latrunculin B on mechanical properties of cells. J. Cell Sci. 114:1025-1036.

21. Danowski, B. A. 1989. Fibroblast Contractility and Actin Organization are Stimulated by Microtubule Inhibitors. J. Cell Sci. 93:255-266.

22. Nye, J. 1985. Physical Properties of Crystals. Oxford University Press, Oxford, UK.

23. Radmacher, M. 1997. Measuring the elastic properties of biological samples with the AFM. IEEE Eng. Med. Biol. Mag. 16:47-57.

24. Wu, H. W., T. Kuhn, and V. T. Moy. 1998. Mechanical properties of l929 cells measured by atomic force microscopy: Effects of anticytoskeletal drugs and membrane crosslinking. Scanning 20:389-397.

25. Haga, H., S. Sasaki, K. Kawabata, E. Ito, T. Ushiki, and T. Sambongi. 2000. Elasticity mapping of living fibroblasts by AFM and immunofluorescence observation of the cytoskeleton. Ultramicroscopy 82:253-258.

26. Berdyyeva, T. K., C. D. Woodworth, and I. Sokolov. 2005. Human epithelial cells increase their rigidity with ageing in vitro: direct measurements. Phys. Med. Biol. 50:81-92.

27. Shin, D., and K. Athanasiou. 1999. Cytoindentation for obtaining cell biomechanical properties. J. Orthop. Res. 17:880-890.

28. Charras, G. T., and M. A. Horton. 2002. Determination of cellular strains by combined atomic force microscopy and finite element modeling. Biophys. J. 83:858-879.

29.Mahaffy, R. E., S. Park, E. Gerde, J. Kas, and C. K. Shih. 2004. Quantitative analysis of the viscoelastic properties of thin regions of fibroblasts using atomic force microscopy. Biophys. J. 86:1777-1793.

30.Trickey, W. R., F. P. T. Baaijens, T. A. Laursen, L. G. Alexopoulos, and F. Guilak. 2006. Determination of the Poisson's ratio of the cell: recovery properties of chondrocytes after release from complete micropipette aspiration. J. Biomech. 39:78-87.

31. Ma, G., E. Petersen, K. W. Leong, and K. Liao. 2012. Mechanical behavior of human embryonic stem cell pellet under unconfined compression. Biomech. Model. Mechanobiol. 11:703-714.

32. Evans, E., and B. Kukan. 1984. Passive Material Behaviour of Granulocytes Based on Large Scale Deformation and Recovery after Deformation Tests. Blood 64:1028-1035.

33. Henon, S., G. Lenormand, A. Richert, and F. Gallet. 1999. A new determination of the shear modulus of the human erythrocyte membrane using optical tweezers. Biophys. J. 76:1145-1151.

34.Kundu, T., J. Bereiterhahn, and K. Hillmann. 1991. Measuring Elastic Properties of Cells by Evaluation of Scanning Acoustic Microscopy V(z) Values using Simplex Algorithm. Biophys. J. 59:1194-1207.

35.Bamber, M. J., K. E. Cooke, A. B. Mann, and B. Derby. 2001. Accurate determination of Young's modulus and Poisson's ratio of thin films by a combination of acoustic microscopy and nanoindentation. Thin Sol. Films 398:299-305.

36. Goodman, O., and B. Derby. 2011. The mechanical properties of float glass surfaces measured by nanoindentation and acoustic microscopy. Acta Mater. 59:1790-1799.

37. Zhao, X., R. Akhtar, N. Nijenhuis, S. J. Wilkinson, L. Murphy, C. Ballestrem, M. J. Sherratt, R. E. B. Watson, and B. Derby. 2012. Multi-Layer Phase Analysis: Quantifying the Elastic Properties of Soft Tissues and Live Cells with Ultra-High-Frequency Scanning Acoustic Microscopy. IEEE Trans. Ultrason. Ferroelec. Freq. Control 59:610-620.

38.Riveline, D., E. Zamir, N. Q. Balaban, U. S. Schwarz, T. Ishizaki, S. Narumiya, Z. Kam, B. Geiger, and A. D. Bershadsky. 2001. Focal contacts as mechanosensors: Externally applied local mechanical force induces growth of focal contacts by an mDia1-dependent and ROCK-independent mechanism. J. Cell Biol. 153:1175-1185.

39.Burridge, K., and K. Wennerberg. 2004. Rho and Rac take center stage. Cell 116:167-179.

40. Schindelin, J., I. Arganda-Carreras, E. Frise, V. Kaynig, M. Longair, T. Pietzsch, S. Preibisch, C. Rueden, S. Saalfeld, B. Schmid, J.-Y. Tinevez, D. J. White, V. Hartenstein, K. Eliceiri, P. Tomancak, and A. Cardona. 2012. Fiji: an open-source platform for biological-image analysis. Nat. Methods 9:676-682.

41.Hutter, J. L., and J. Bechhoefer. 1993. Calibration of atomic-force microscope tips. Rev. Sci. Instrum. 64:3342-3342.

42. Fischer-Cripps, A. C. 2000. A review of analysis methods for sub-micron indentation testing. Vacuum 58:569-585.

43.Citi, S., and J. Kendrickjones. 1986. Regulation in vitro of Brush-Border Myosin by Light Chain Phosphorylation. J. Mol. Biol. 188:369-382.

44. Wilkinson, S., H. F. Paterson, and C. J. Marshall. 2005. Cdc42-MRCK and Rho-ROCK signalling cooperate in myosin phosphorylation and cell invasion. Nat. Cell Biol. 7:255-U245.

45. Watanabe, N., T. Kato, A. Fujita, T. Ishizaki, and S. Narumiya. 1999. Cooperation between mDia1 and ROCK in Rho-induced actin reorganization. Nat. Cell Biol. 1:136-143.

46.Uehata, M., T. Ishizaki, H. Satoh, T. Ono, T. Kawahara, T. Morishita, H. Tamakawa, K. Yamagami, J. Inui, M. Maekawa, and S. Narumiya. 1997. Calcium sensitization of smooth muscle mediated by a Rho-associated protein kinase in hypertension. Nature 389:990-994.

47. Rapoport, N. Y., A. L. Efros, C. D. A, K. A. M, and N. K. H. 2009. Microbubble generation in phase-shift nanoemulsions used as anticancer drug carriers. Bubble Sci. Eng. Technol. 1:31-39.

48.Baddour, R. E., M. D. Sherar, J. W. Hunt, G. J. Czarnota, and M. C. Kolios. 2005. High-frequency ultrasound scattering from microspheres and single cells. J. Acoust. Soc. Am. 117:934-943.

49. Taggart, L. R., R. E. Baddour, A. Giles, G. J. Czarnota, and M. C. Kolios. 2007. Ultrasonic characterization of whole cells and isolated nuclei. Ultrasound Med. Biol. 33:389-401.

50.Kaufman, J. D., G. J. Miller, E. F. Morgan, and C. M. Klapperich. 2008. Time-dependent mechanical characterization of poly(2-hydroxyethyl methacrylate) hydrogels using nanoindentation and unconfined compression. J. Mater. Res. 23:1472-1481.

51.Alcaraz, J., L. Buscemi, M. Puig-de-Morales, J. Colchero, A. Baro, and D. Navajas. 2002. Correction of microrheological measurements of soft samples with atomic force microscopy for the hydrodynamic drag on the cantilever. Langmuir 18:716-721.

52. Levy, R., and M. Maaloum. 2002. Measuring the spring constant of atomic force microscope cantilevers: thermal fluctuations and other methods. Nanotechnology 13:33-37.

53. Kuznetsova, T. G., M. N. Starodubtseva, N. I. Yegorenkov, S. A. Chizhik, and R. I. Zhdanov. 2007. Atomic force microscopy probing of cell elasticity. Micron 38:824-833.

54. Anderson, E. C., D. F. Petersen, and R. A. Tobey. 1970. Density invariance of cultured chinese hamster cells with stage of mitotic cycle. Biophys. J. 10:630-636.

55.Grover, W. H., A. K. Bryan, M. Diez-Silva, S. Suresh, J. M. Higgins, and S. R. Manalis. 2011. Measuring single-cell density. Proc. Nat. Acad. Sci. U.S.A. 108:10992-10996.

56.Tschoegl, N. W., W. G. Knauss, and I. Emri. 2002. Poisson's ratio in linear viscoelasticity - A critical review. Mech. Time-Depend. Mater. 6:3-51.

57. Mizuno, D., C. Tardin, C. F. Schmidt, and F. C. MacKintosh. 2007. Nonequilibrium mechanics of active cytoskeletal networks. Science 315:370-373.

58.Ishizaki, T., Y. Morishima, M. Okamoto, T. Furuyashiki, T. Kato, and S. Narumiya. 2001. Coordination of microtubules and the actin cytoskeleton by the Rho effector mDia1. Nat. Cell Biol. 3:8-14.

59. Wagner, O., J. Zinke, P. Dancker, W. Grill, and J. Bereiter-Hahn. 1999. Viscoelastic properties of f-actin, microtubules, f-actin/alpha-actinin, and f-actin/hexokinase determined in microliter volumes with a novel nondestructive method. Biophys. J. 76:2784-2796.

60. Hull, D., and T.W. Clyne. 1996. An Introduction to Composite Materials. Cambridge University Press, Cambridge, U.K.

61.Chang, Y.-C., P. Nalbant, J. Birkenfeld, Z.-F. Chang, and G. M. Bokoch. 2008. GEF-H1 couples nocodazole-induced microtubule disassembly to cell contractility via RhoA. Mol. Biol. Cell 19:2147-2153.

62. Kelly, G. M., J. I. Kilpatrick, M. H. van Es, P. P. Weafer, P. J. Prendergast, and S. P. Jarvis. 2011. Bone cell elasticity and morphology changes during the cell cycle. J. Biomech. 44:1484-1490.

63. Maniotis, A. J., C. S. Chen, and D. E. Ingber. 1997. Demonstration of mechanical connections between integrins cytoskeletal filaments, and nucleoplasm that stabilize nuclear structure. Proc. Nat. Acad. Sci. U.S.A. 94:849-854.

Figure Captions

Figure 1 Schematic diagram, after Riveline et al (21), showing the effect of Rho on cell mechanical properties through the activation of two pathways: ROCK dependent and mDia1 dependent. The ROCK dependent pathway tensions the actin fibres through myosin II–driven cell contractility either directly or indirectly, via myosin light chain phosphatase (MLCP). The mDia1 dependent pathway activates actin polymerization, or possibly influences the organization of the actin network and microtubules.

Figure 2 SAM and AFM experiments on populations of cells treated with Y-27632 and a control population. a) Filamentous actin structure in a control NIH3T3 cell showing regular straight, tensioned filaments called stress fibres. b) Highly disorganised actin filamentary structure observed after treatment with Y-27632. c) SAM image showing characteristic interference rings from a typical control NIH3T3 cell. d) NIH32T3 cell after treatment with Y-27632 showing a larger number of interference rings and a more raised profile. In all images the scale bar indicates 10 μm. e) Mean (± S.E.) acoustic wave velocity (control: n = 27, Y-27632: n = 51) and contact elastic modulus (control: n = 92: Y-27632: n = 27). f) Computed bulk modulus (K) and shear modulus (G). In all cases * indicates a statistically significant difference ($P < 0.05$) between treated and control populations.

Figure 3 SAM and AFM experiments on populations of cells transfected with mDia1ΔN3 and a control population. a) NIH3T3 cell transfected with mDia1ΔN3 packed with a dense network of actin stress fibres; scale bar indicates 10 μm. b) SAM image showing interference rings from transfected NIH3T3 cells; scale bar indicates 20 μm. c) Mean ± S.E. acoustic wave velocity (control: n = 38, mDia1ΔN3: n = 45) and contact elastic modulus (control: n = 30, mDia1ΔN3: n = 55). d) Computed Mean ± SE bulk modulus (K) and shear modulus (G). In all cases * indicates a statistically significant difference ($P < 0.05$) between treated and control populations.

Figure 4 SAM and AFM experiments on populations of NIH3T3 cells treated with nocodazole and a control population. a) NIH3T3 cell in control condition stained to reveal microtubules. b) After treatment with nocodazole the microtubule structure is no longer revealed by the stain, indicating severe disruption. c) NIH3T3 cell in control condition stained to reveal actin. d) After treatment with nocodazole, actin filaments are clearly present in a similar amount to the control and well aligned. In images a-d the scale bars indicate 10 μm. e) SAM image of the cells after treatment with nocodazole, the presence of several interference rings show that the cells have maintained a 3D shape; scale bar indicates 20 μm. f). Mean (± S.E.) acoustic wave velocity (control: n = 34, nocodazole: n = 47) and contact elastic modulus (control: n = 39, nocodazole: n = 40). g) Computed mean ± S.E. bulk modulus (K) and shear modulus (G). In all cases * indicates a statistically significant difference ($P < 0.05$) between treated and control populations.

Figure 5 Deviation of the value of Poisson's ratio from the incompressible limit ($\nu = 0.5$) for the cell populations studied after a number of treatments.